

Nanoscale

Accepted Manuscript



This is an *Accepted Manuscript*, which has been through the Royal Society of Chemistry peer review process and has been accepted for publication.

Accepted Manuscripts are published online shortly after acceptance, before technical editing, formatting and proof reading. Using this free service, authors can make their results available to the community, in citable form, before we publish the edited article. We will replace this *Accepted Manuscript* with the edited and formatted *Advance Article* as soon as it is available.

You can find more information about *Accepted Manuscripts* in the [Information for Authors](#).

Please note that technical editing may introduce minor changes to the text and/or graphics, which may alter content. The journal's standard [Terms & Conditions](#) and the [Ethical guidelines](#) still apply. In no event shall the Royal Society of Chemistry be held responsible for any errors or omissions in this *Accepted Manuscript* or any consequences arising from the use of any information it contains.

Synthesis, characterization, and biodistribution of multiple ^{89}Zr -labeled pore-expanded mesoporous silica nanoparticles for PET

Larissa Miller,¹ Gordon Winter,² Benjamin Baur,² Barbara Witulla,² Christoph Solbach,² Sven Reske,^{2,*} Mika Lindén^{1,*}

¹ Department of Inorganic Chemistry II, University of Ulm, Albert-Einstein-Allee 11, D-89081 Ulm, Germany

² Clinic for Nuclear Medicine, University of Ulm, Albert-Einstein-Allee 23, D-89081 Ulm, Germany

Corresponding author e-mail addresses: mlinden@uni-ulm.de, sven.reske@uniklinik-ulm.de

Abstract

Functional nanoparticles are highly interesting imaging agents for positron emission tomography (PET) due to the possibility of multiple incorporation of positron emitting radionuclide thus increasing the signal strength. Furthermore, longer-term nanoparticle biodistribution tests with increased signal-to-noise ratio can be achieved with nanoparticles carrying long-lived isotopes. Mesoporous silica nanoparticles, MSNs, have attracted a lot of recent interest as both imaging agents and carriers for drugs *in vitro* and *in vivo*. Here we present results related to the synthesis of PET imagable MSNs carrying the long-lived $^{89}\text{Zr}^{4+}$ isotope (half-life of 78.4 hours). Here, $^{89}\text{Zr}^{4+}$ was immobilized through covalent attachment of the complexing agent p-isothiocyanatobenzylferrioxamine B (DFO-NCS) to large-pore MSNs. Due to the high DFO content of the MSNs, the $^{89}\text{Zr}^{4+}$ labeling was quantitatively within just a few minutes, and no subsequent purification step was needed in order to remove non-complexed $^{89}\text{Zr}^{4+}$. Stability of the ^{89}Zr -labeled MSNs against leaching of $^{89}\text{Zr}^{4+}$ was verified for 24 hours. The high signal strength of the ^{89}Zr -DFO-MSNs was evidenced by successful PET imaging using a mouse model at particle loadings one order of magnitude lower than those previously applied in PET-MSN studies. The biodistribution followed the same trends as previously observed for MSNs of different size and surface functionality.

Taken together, our results suggest that ^{89}Zr -DFO-MSNs are promising PET imaging agents for longer-term *in vivo* imaging.

Introduction

Mesoporous silica nanoparticles (MSNs) have emerged as a promising and flexible platform for therapeutic and diagnostic applications. For recent reviews see for example.¹⁻⁶ An ever increasing number of *in vitro* and *in vivo* studies show that MSNs are generally biocompatible, degrade in biological environments, and are cleared from the body mainly through renal clearance.^{7, 8} The possibility for independent control of key-parameters like particle and pore size and shape, and surface properties, are other attractive characteristics for using MSNs in biological applications. The particle size control is very important in order to optimize MSNs for different forms of administration, as the optimum particle size is highly administration route dependent. Furthermore, the high internal surface area and pore volumes of MSNs, together with the possibility to tune the pore dimension and surface chemistry of the mesopores makes it possible to load large amount of cargo, and also to tune the interactions between the cargo and the carrier. This allows the MSNs to be optimized for a given application, and also opens up the possibility for creating multifunctional particles. There are many examples in the literature of MSNs that have been applied both as drug carriers and imaging agents, thus combining therapeutics and diagnostics often referred to as theranostics, as summarized in a number of recent reviews.^{9, 10} The biodistribution can be further influenced through covalent linking of targeting agents to the outer surface of the MSNs. A highly selective accumulation of MSNs in solid tumours has been shown *in vivo* in mice models for MSNs tagged with targeting ligands as proven both by live animal imaging and *ex vivo* organ analyses.¹¹ Not surprisingly, most of the current research related to MSNs for therapeutic use is therefore focused on chemotherapy-related applications. However, the potential for clinical application using MSNs as imaging agents is also receiving increasing attention. PET allows semi-quantitative biodistribution studies *in vivo*, and close-to-quantitative organ distribution profiles can be obtained by *ex vivo* organ analyses. Furthermore, PET is also the method of use for diagnostics. The most clinically applied PET-active isotope is ^{18}F , typically in the form of ^{18}F -labeled fluorodeoxyglucose in order to target the tracer to high-glucose-using cells such as brain, kidney and cancer cells. However, the half-life of ^{18}F is only 109.8 minutes, which puts a limit to the maximum observation time for single administration. A relevant improvement would therefore be the development of MSN-

based carriers for the application of positron emitting radionuclides with longer half-lives $t_{1/2}$. In combination with the possibility of multiple labeling on a single carrier this would allow for longer-term, PET imaging with a single administration at low particle doses. In addition to longer-term nanoparticle biodistribution studies, such particles are also interesting for following sub-populations of cells in the body over time. There are a few reports where radiolabeled MSNs have been studied *in vivo*, either using ^{124}I or ^{64}Cu as the radionuclide, which have demonstrated the high promise of such particles for biodistribution studies.¹²⁻¹⁵ The half-life of ^{64}Cu is 12.7 hours and that of ^{124}I is about 100.2 hours, which is why these isotopes are more interesting for longer-term PET imaging as compared to ^{18}F . However, in most of the above described cases, the complexing agent for the PET radionuclides has been located on the outer surface of the MSNs, except for the study by Huang et al.¹⁴ This limits the maximum loading degrees, and thus the signal strength of the particles. Therefore, MSNs having the possibility to carry a higher number of PET active isotopes would be especially interesting for long-term biodistribution studies, as these studies could then also be carried out at low particle concentrations without compromising the data quality. In the present communication we demonstrate successful preparation of stable and multiple ^{89}Zr -labeled MSNs which are dispersible in biological media, and where quantitative complexation of ^{89}Zr can be achieved on a time-scale of minutes. Furthermore, no leaching of radionuclide from the MSNs was observed. Biodistribution studies were performed using a nude mouse model carrying a prostate cancer tumour, and clear differences were observed between the biodistribution of the ^{89}Zr -MSNs as compared to free $^{89}\text{ZrCl}_4$. The high signal strength of the ^{89}Zr -MSNs allowed us to obtain high-quality images *in vivo* at MSN concentrations an order of magnitude lower than those used in previous studies using PET-active MSNs.

Experimental

Materials

Tetramethyl orthosilicate (TMOS), 3-aminopropyltrimethoxysilane (APTMS), dimethylsulfoxide (DMSO) were obtained from Sigma-Aldrich (Steinheim, Germany). Cetyltrimethylammonium bromide (CTAB), methanol, sodium hydroxide, toluene, ammonium nitrate and trioctylphosphine oxide (TOPO) were purchased from Merck (Hohenbrunn, Germany). p-Isothiocyanatobenzylferrioxamine B (DFO-NCS) was bought from Macrocyclics (Dallas, USA). All reagents and solvents were the highest grade available and used without further purification.

Materials characterization

The nitrogen sorption isotherms (77 K) were obtained using a Quadrasorb SI setup (Quantachrome). The samples were outgassed at 140°C for 8 h before the measurements. Surface area calculations were made using the BET method. Pore-size distributions and pore-volumes were calculated according to the NLDFIT method applying the kernel developed for cylindrical pores. Particle morphology was determined by scanning electron microscopy using a Hitachi S-5200 FE-SEM system with 20 kV accelerating voltage. Transmission electron microscopy (TEM) studies were carried out on a Zeiss EM 10 instrument operated at 80 kV. Therefore samples were embedded in epoxy resin and then cut in thin slices (80 – 100 nm) attached on carbon-coated copper grids. Hydrodynamic particle size, particle size distributions, and zeta potentials in 100 mM KCl (pH = 7, 25°C) solution were measured on a Malvern Zetasizer Nano ZS. The C,H,N-analyses was performed using a Vario El instrument. The absorption spectra of the chelator were measured using a Nanodrop 2000c UV-VIS spectrophotometer at a wave-length of 281 nm.

Synthesis of pore-expanded MSNs

The pore-expanded mesoporous silica nanoparticles were synthesized using the procedure described by Kim et al.¹⁶, with the difference that the swelling agent mesitylene (TMB) was replaced by trioctylphosphine oxide (TOPO). In a typical synthesis, 7.2 g of CTAB and 2.4 ml of 2 M sodium hydroxide solution were dissolved in a mixture of methanol and water (1600 g, 40:60, w/w). Under vigorous stirring at 25°C 2.6 ml TMOS was added to the solution. The molar composition was 1 TMOS: 1.12 CTAB: 0.27 NaOH: 1135 methanol: 3028 H₂O. After 8 h of continuous stirring, the mixture was aged overnight. The precipitate was obtained by centrifugation and washed with ethanol two times. Before centrifugation the particles were flocculated using NH₄NO₃. The pore-expansion was achieved through a postsynthesis hydrothermal treatment in the presence of TOPO and a small amount of NH₄NO₃. The surfactant-containing nanoparticles were dispersed in ethanol by sonication for 1 h, following by the addition of a solution of 1g TOPO in ethanol/water (1:1, v/v). The mixture was sealed in a vessel and heated in an autoclave at 398 K for 3 days without stirring. The resulting particles were centrifuged and washed with ethanol. The surfactant was removed by ultrasonication in a solution of concentrated hydrochloric acid in ethanol (5 g/l) three times.

Amino-Functionalization

The extracted particles were dispersed in toluene followed by the addition of APTMS in a molar ratio of 5 SiO₂/1 APTMS. The mixture was refluxed overnight, centrifuged and washed two times in ethanol.

Conjugation with DFO-NCS

DFO-NCS was dissolved in anhydrous DMSO (8 mg/ml) for 5 min until a clear solution was formed. Pore-expanded amino-labeled silica particles (30 mg) were added into the DFO solution. The reaction solution was kept at 40 °C for 24 h to allow the reaction between amino groups on the particle surface and isothiocyanate groups to complete. The resulting product was cleaned by centrifugation and redispersion in DMSO and ethanol to remove excess or unreacted DFO molecules. The amount of DFO was calculated by subtracting the amount found in the supernatant liquid after conjugation from the amount of DFO present before addition of the chelate by UV absorption at 281 nm. The same settings were used for determination of the DFO binding isotherm.

Cyclotron production, separation and purification of zirconium-89

Zirconium-89 ($t_{1/2} = 78.4$ h, β^+ : 23 %, $E_{\beta^+ \text{max}}$, 901 KeV; EC: 77 %, $E_{\gamma \text{max}}$: 909 KeV) was produced by proton bombardment of commercially available, high-purity ⁸⁹Y-foil (25 mm × 12.5 mm × 0.127 mm, approx. 0.33 g, 3.70 mmol) using the ⁸⁹Y(*p,n*)⁸⁹Zr nuclear reaction on a PETtrace cyclotron (GE) as described by Solbach et al.¹⁷

Purification and preparation of ⁸⁹Zr-chloride were done similarly to the procedure described by Holland et al.¹⁸

Radiosynthesis of ⁸⁹Zr-DFO-MSNs

⁸⁹ZrCl₄ with a total activity of 8.0-8.4 MBq (5.41 pmol, 20 μL; pH = 7) was added to a dispersion of DFO-MSNs dissolved in DMSO, and 1 ml 0.25 M NH₄OAc-buffer (pH = 7.7) buffer (pH 7.4, 500 μL) for a total volume between 1025-1070 μL and a final pH of 7.7. Different amounts of nanoparticles (10, 25, 50 and 100 μg) were used for studying the dependence between concentration of DFO-MSNs and RCY of ⁸⁹Zr-DFO-MSNs (n=2). The reaction was carried out at room temperature for 30 min. At different reaction times (1, 5, 15, and 30 min), 1 μL aliquots were withdrawn and analyzed by radio-TLC (0.1 M citrate-buffer; pH 5). Quantification was performed by phosphorimager measurements.

Radio-TLC analysis

To determine dependency of the RCY between time and nanoparticle concentrations of the labeling reaction, samples (1 μ L) were withdrawn at the mentioned times directly from the reaction mixture of labeled DFO-MSNs for radio-TLC analysis. As stationary phase RP-18 Silica gel plates and as mobile phase trisodium citrate dihydrate buffer (0.1 M, pH 5) was used. Under these conditions free radiometal forms a citrate complex and is eluted with the solvent front while ^{89}Zr -DFO-MSNs remain on the starting point. Quantitative assay of radioactive spots was carried out by phosphorimager.

Biodistribution experiments

For xenotransplantation male severe-combined immunodeficiency mice (SCID, Charles River) were inoculated subcutaneously dorsal in the subscapular region with 1×10^6 cells in 0.2 ml media and matrigel (1:1, v/v). Prostate carcinoma cell lines LNCaP C4-2 were used for xenotransplantation.¹⁹ Tumor growth was daily observed by palpation. To avoid the formation of necrotic tissue the tumors were left to grow to a maximum size of 12 x 8 x 5 mm.

Mice were continuously anesthetized using 1.5% isofluran (Abbott) in oxygen. For each injection 10 μ g ^{89}Zr -labeled MSNs (0.5 mg/kg mouse) were applied intravenously to the tail vein at a volume of 0.15 ml. Administration was controlled by measuring the whole mouse in the dose calibrator prior PET and by separate activity quantification of the tail for paravenous injection after sacrifice the animal.

Static images were acquired after 60 up to 240 min post injection using a PET/CT scanner (Biograph mCT, Siemens Healthcare Germany) while animals were continuously anesthetized using 1.5% isoflurane. Tube voltage of the CT was set to 80 kV. Acquisitions time took 62.7 seconds at a rotation time of one second. Data were collected with a pitch of 0.55, a slice thickness of 0.6 mm and were reconstructed with kernel H70s (Siemens Healthcare).

PET measurements were performed at one bed position for 10 min. For PET reconstruction CT based attenuation correction and the iterative algorithm with 4 iteration and 21 subsets was used. The images were filtered by Gauss filter with FWHM (full width of half maximum) of 1 mm. Images have been evaluated using the Syngo.Via with the MM Oncology package (Siemens Healthcare) while the overlay images were prepared using Adobe Photoshop CS6.

Blood was collected immediately after sacrifice (cervical dislocation) and selected tissues were harvested, weighed and counted in an automated gamma counter (Packard COBRA II, Perkin-Elmer). Tissue radiopharmaceutical uptake values were calculated as percent injected dose per gram (%ID/g).

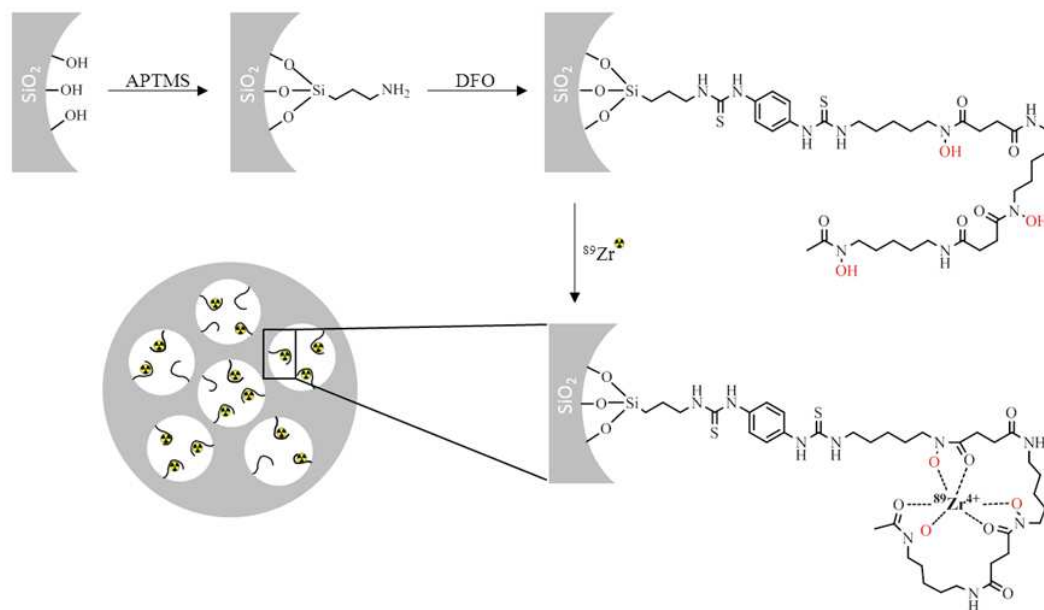


Figure 1. A schematic representation of MSNs functionalized with APTMS, coupled with DFO and radiolabeled with radionuclide ^{89}Zr .

Results and discussion

In this preliminary study, we chose to work with spherical MSNs with a mean diameter of about 180 nm, as MSNs in this size range have successfully been applied *in vivo*. As discussed above, one of the key-properties of high-resolution PET imaging using nanoparticles is the high label stability over time. One of the best chelators known for $^{89}\text{Zr}^{4+}$ is the poorly water soluble deferoxamin (DFO), also known as Desferal[®].²⁰ We therefore synthesized MSNs where DFO was covalently linked to the particles, as schematically shown in Figure 1. Initial studies showed that DFO could not be introduced to standard MSNs at high loadings, which we assigned to the relatively small pore size of 3-4 nm of these MSNs. In order to increase the pore size of the MSNs without affecting the particle size, we performed hydrothermal post-treatment of the as-synthesized, particles still containing some of the surfactant, in an ethanol-water-trioctylphosphine oxide (TOPO) solution for three days at 125°C. Nitrogen sorption isotherms measured for non-hydrothermally treated and hydrothermally treated MSNs and the corresponding pore size distributions are shown in Figure 2. Hydrothermal treatment leads to a clear shift of the relative pressure range within which pore filling of intra-particle mesopores occurs, suggesting that the hydrothermal treatment indeed leads to an increase in the mesopore size. The relative pressure range within which capillary condensation occurs inside the intra-particle mesopores of the

hydrothermally treated MSNs is relatively broad, suggesting a broad mesopore size distribution. However, the narrow hysteresis gives evidence for a mesopore system where the mesopores are not connected through smaller mesopores, which otherwise could lead to diffusion limitations during the loading step. The mean pore dimension increases from 3.5 nm to 8 nm upon hydrothermal treatment (see Figure 2), but the pore size distribution is broader for the hydrothermally treated particles. At the same time, the pressure range for condensation of nitrogen within interparticular mesopores occurring at high relative pressures is the same for both native and hydrothermally treated particles, indicating that the mean particle diameter is not affected by the hydrothermal treatment. The adsorbed amount of nitrogen in the low pressure regime is clearly lower for the hydrothermally treated sample, suggesting loss of surface area and potential microporosity upon hydrothermal treatment. This is also reflected in the calculated specific surface areas, which decreased from 1236 m²/g to 407 m²/g upon hydrothermal treatment. However, the volume of nitrogen adsorbed during the filling of the internal mesopores was virtually identical in the two cases, indicating that there was limited loss of primary mesopore volume during the hydrothermal treatment step. The primary mesopore volume of the hydrothermally treated sample was 0.62 ml/g.

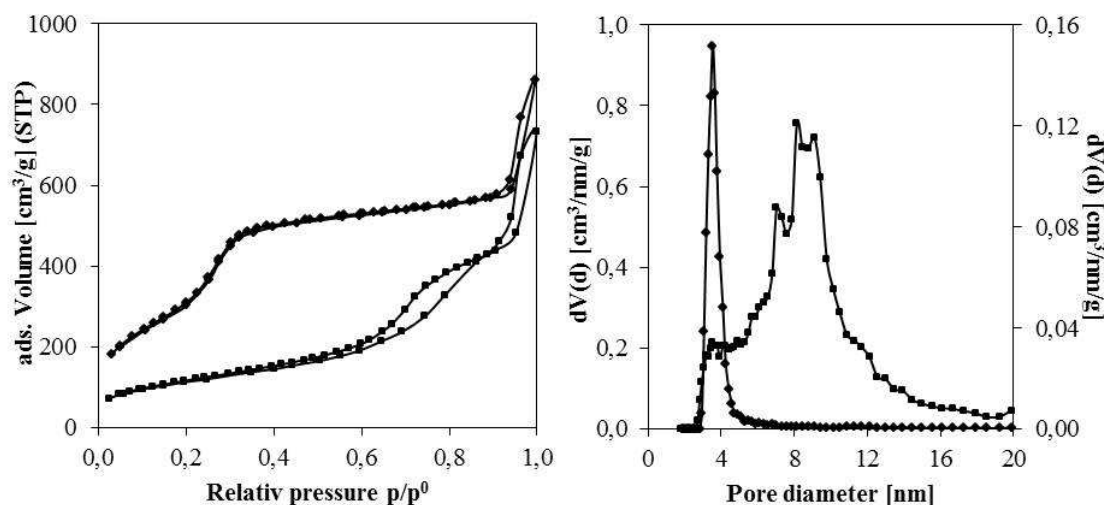


Figure 2. Nitrogen adsorption-desorption isotherms (left) and pore size distribution (right) of original MSN (◆) and pore-expanded MSN (■) samples.

SEM images of native and hydrothermally treated MSNs are shown in Figure 3. As stated above, the mean particle size of the native particles was 180 nm, with a relatively narrow particle size distribution. The same is true for the hydrothermally treated particles, but the hydrothermal treatment leads to a roughening of the MSNs surface, while the mean particle

size remains virtually unchanged which is also true for the particle shape. Thus, the particle size analyses based on SEM is in good agreement with the conclusions based on analyses of the nitrogen sorption data. The pronounced change in the micro-morphology of the particles upon hydrothermal treatment is a consequence of dissolution and re-precipitation of silica during the hydrothermal conditions. Importantly, there are evidently no bridged particles to be seen, suggesting that the dissolution-re-precipitation process does not lead to precipitation of silica in the neck-region between particles. This is an absolute key-criterion for dispersibility of the particles for further application in biological systems.

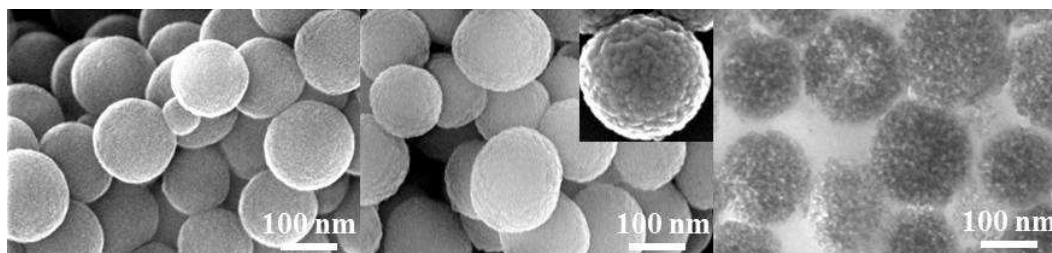


Figure 3. SEM images of non-expanded (left) and pore-expanded (in the middle) MSNs including a close-up view of a particle and a related TEM image (right).

A TEM image taken of microtomed particles after hydrothermal treatment is also shown in Figure 3. It is evident that the mesopores are homogeneously distributed throughout the particles.

The hydrothermally treated MSNs were post-functionalized with APTMS in order to introduce anchoring groups for DFO. Based on C,H,N-analyses, a total APTMS loading degree of 1.5 mmol/m^2 was obtained, which was in good agreement with thermogravimetric analysis. (See ESI) The zeta-potential measured at $\text{pH} = 7$ and a background electrolyte concentration of 100 mM KCl increased from a value of close to 0 mV measured for the native, hydrothermally treated MSNs to about $+35 \text{ mV}$ upon APTMS functionalization, which is another indication for a successful introduction of amino-groups onto the hydrothermally treated MSNs. (See ESI)

The linking of DFO to the amino-functionalized hydrothermally treated MSNs was performed in a solution of isothiocyanate-functionalized DFO in DMSO. The isothiocyanate is covalently attached to amino-groups present on the MSNs under formation of a thiourea group. The loading was studied as a function of DFO concentration, and the results are

summarized in Figure 4. A plateau was reached at about 250 $\mu\text{mol DFO/g silica}$, corresponding to 1.42 $\mu\text{mol/m}^2$ silica, when the initial concentration of DFO in DMSO was about 8 mg/ml. A further increase in the DFO concentration in DMSO did not lead to a higher DFO loading. The maximum loading capacity was also confirmed by thermogravimetric and elemental analysis. (See ESI) Nitrogen sorption analyses of the non-functionalized and DFO-functionalized MSNs show a decrease in the specific pore volume upon DFO loading even if the increased mass of the DFO-loaded particles is taken into account. However, the fact that an appreciable pore volume was still observed suggest that there is a distribution of DFO between the outer and the inner surfaces of the MSNs. (See ESI) Particles having the maximum loading reached under the studied conditions were chosen for further labeling with ^{89}Zr . As expected, the zeta-potential value measured at pH = 7 and at a KCl concentration of 100 mM decreased from +35 mV observed for the amino-functionalized MSNs to +16 mV upon DFO binding. (See ESI) Adsorption of Zr^{4+} to the DFO-MSNs from an aqueous ZrCl_4 solution having the same concentration as in the PET experiments (see later) did not lead to any further changes in the zeta-potential value. This is to be expected if the adsorption of Zr^{4+} only occurs to the DFO complex, as 4 protons would be exchanged against a tetravalent Zr-ion. Thus, this result confirms the high adsorption selectivity of our MSNs.

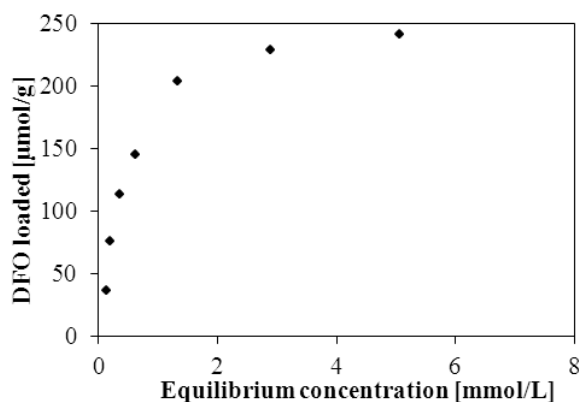


Figure 4. DFO binding isotherm to MSNs from DMSO using chelator concentrations 1-10 mg/mL.

Before labeling of the DFO-MSNs with $^{89}\text{Zr}^{4+}$, we confirmed that the particles were dispersible. This is especially important as any DFO attached to the outer surface of the particles could make them less dispersible in aqueous media due to increased particle hydrophobicity. Determination of the hydrodynamic particle diameters was performed by dynamic light scattering, DLS, in 100 mM KCl solution at pH 7 for hydrothermally treated MSNs at different stages of the functionalization. The dispersibility of the DFO-MSNs was

also confirmed in 10 % fetal calf serum (FCS). The results are shown in Figure 5. The results imply that a) the DFO-functionalized particles are as dispersible as the native and amino-functionalized particles, b) the particle size distribution remains narrow in all cases, and c) the particle size determined by DLS is in good agreement with the particle size determined by SEM.

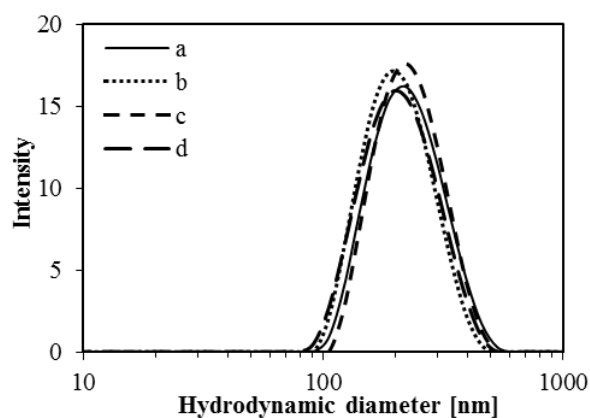


Figure 5. Hydrodynamic diameters determined for hydrothermally treated MSNs at different stages of the functionalization process; a) native particles, b) amino-functionalized particles, and c-d) DFO-functionalized particles. The particle concentration was 100 $\mu\text{g/ml}$ in all cases and the measurements a)-c) were carried out in a 100 mM KCl solution at pH 7, d) was measured in cell culture media with 10 % FCS.

In order to optimize the concentration of PET active ^{89}Zr -DFO-MSN, the labeling reaction was studied as a function of time and DFO-MSN concentration. This is an important parameter, as it is to be expected that the ^{89}Zr labeling increases with time (diffusion limitations), but at the same time the activity of ^{89}Zr decreases with time. Furthermore, a quantitative labeling reaction with $^{89}\text{Zr}^{4+}$ eliminates the need for a subsequent washing step eliminating non-bound $^{89}\text{Zr}^{4+}$. $^{89}\text{Zr}^{4+}$ with a total activity of 8.0-8.4 MBq was added to dispersions of MSNs at different concentrations. At particle concentrations exceeding 50 mg/L complete incorporation of $^{89}\text{Zr}^{4+}$ was observed within 3 minutes. The corresponding values were 15 min and 30 min for particle concentrations of 25 mg/L and 10 mg/L. (See ESI) Thus, the activity per particle can be varied within a relatively broad range, still achieving virtually complete complexation of $^{89}\text{Zr}^{4+}$ by DFO-MSNs. These results stand in contrast to previous studies, which is why an additional purification step is needed in their case.^{12, 14, 15} The dispersibility of the ^{89}Zr -DFO-MSNs in FCS was studied as a function of time using PET. (See Figure 6 and ESI) The dispersions were stable over at least 60 minutes, which is more than sufficient in order to ensure that fully dispersed ^{89}Zr -DFO-MSNs can be

administered under clinical conditions. The decrease in activity within one hour was 1.2 % in media with FCS (fetal calf serum). (See ESI)

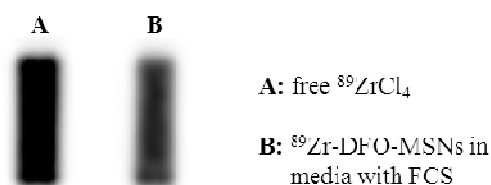


Figure 6. Phantom images of ⁸⁹ZrCl₄ solution (3.5 MBq) and a dispersion of radiolabeled MSNs (10 mg/L, 1.9 MBq) over time for the first 30 minutes.

The time-dependent stability of the ⁸⁹Zr-DFO-MSNs was studied by thin layer chromatography up to 24 h. Stability of ⁸⁹Zr-DFO-MSNs was demonstrated within this time frame (see Figure 7), which is instrumental for allowing the true biodistribution of the MSNs to be followed over time.

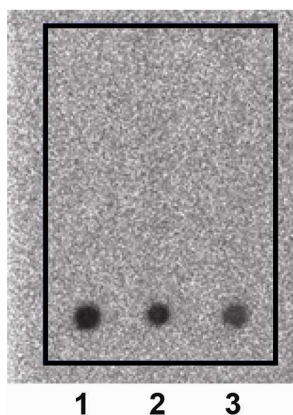


Figure 7. Thin layer chromatography of ⁸⁹Zr-DFO-MSN after 24 h of incubation in FCS. No separation of free ⁸⁹Zr⁴⁺ was observed, giving proof for the stability of the ⁸⁹Zr-DFO-MSNs.

⁸⁹Zr-DFO-MSNs with a total activity of 5 MBq (100 mg/L DFO-MSNs was used during the radiolabeling) were injected into the tail vein of mice bearing a prostate cancer tumour (LNCaP C4-2) in the subscapular region. The particle concentration was 0.5 mg/kg mice, which is about an order of magnitude lower than what to date has been used for PET-MSN biodistribution analyses, and more than an order of magnitude lower than those used when other means for analyses, like ICP, have been used.²¹⁻²³ Even under these conditions, the particles were giving a strong PET signal *in vivo*, as seen in the PET-CT images shown in Figure 8 taken 1 h after injection. The results were compared with corresponding images

obtained when $^{89}\text{Zr}^{4+}$ was administered as a salt solution, and these images are also shown in Figure 8.

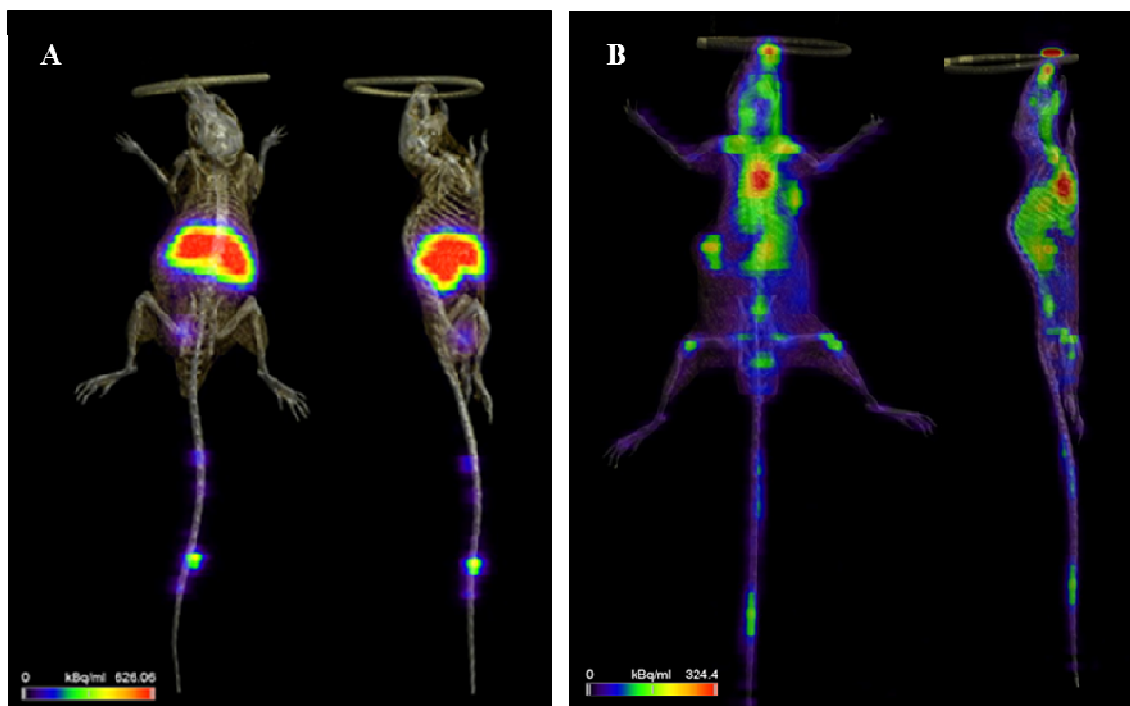


Figure 8. PET image co-registered with the corresponding CT image (Siemens Biograph mCT) of mice taken 1 h after injection into the tail vein. (A) ^{89}Zr -DFO-MSNs and (B) $^{89}\text{ZrCl}_4$ solution. The particle concentration was 0.5 mg/kg mouse and the total initial activity was 5.5 MBq. Images have been evaluated using the Syngo.Via with the MM Oncology package (Siemens Healthcare).

While the ^{89}Zr -DFO-MSNs accumulated mainly in the heart, liver, and spleen, $^{89}\text{Zr}^{4+}$ administered in free form was distributed over the whole body. The quantified distributions of $^{89}\text{Zr}^{4+}$ in the two cases are shown in Figure 9. In addition to the lung, liver, and spleen, the MSNs were also found in the kidney and in the tail, albeit at much lower concentrations. In contrast, the free $^{89}\text{Zr}^{4+}$ was present largely in the blood, and also distributed relatively homogeneously over all main organs. This was also true for the tumour, where little or no accumulation of MSNs was observed. However, the MSNs were not optimized for maximum tumour uptake, and further surface functionalization of the MSNs could be done in order to improve the biodistribution. These results are in good agreement with previous reports on the biodistribution of MSNs, where an initial accumulation in liver, spleen, and lungs has been found virtually independent of the particle size and the surface functionalization.²⁴ Other studies²¹ have also shown the presence of MSNs in the kidney at levels higher than what we observe for the ^{89}Zr -DFO-MSNs, which we ascribe to a combination of larger particle

dimensions in our case, combined with a more hydrophobic nature of DFO-MSNs as compared to “naked” MSNs, also implying a slower hydrolytic degradation in the case of the DFO-MSNs. We also ascribe the higher total accumulations in liver, spleen, and lungs to the same reasons. The different distribution observed for $^{89}\text{Zr}^{4+}$ when administered as ^{89}Zr -DFO-MSNs as compared to the salt form also imply that the stability of the ^{89}Zr -DFO-MSNs observed *in vitro* is also mirrored *in vivo*. These preliminary *in vivo* results demonstrate that the ^{89}Zr -DFO-MSNs are highly promising imaging agents for long-term biodistribution studies. Further optimization possibilities include particle size and shape variations as well as additional surface functionalization, a work which is currently underway in our laboratories.

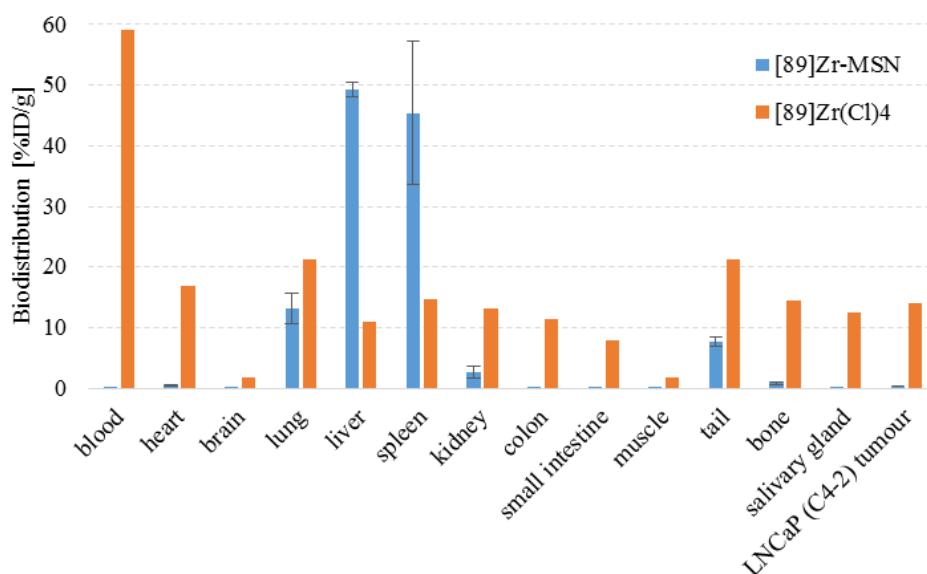


Figure 9. Biodistribution of ^{89}Zr -DFO-MSNs as compared to $^{89}\text{ZrCl}_4$ in salt form. The mice were sacrificed 1 h after intravenous administration into the tail vein. The particle concentration was 0.5 mg/kg mouse.

Conclusions

In this study we have shown that pore-expanded MSNs functionalized with DFO are capable of complexing large amounts of $^{89}\text{Zr}^{4+}$ in a very efficient fashion, eliminating the need for subsequent purification steps after the $^{89}\text{Zr}^{4+}$ labeling. The DFO-MSNs give a high PET signal *in vivo* after quantitative radiolabeling with ^{89}Zr one order of magnitude lower than previously reported. Stability against ^{89}Zr -leaching from the ^{89}Zr -DFO-MSNs was proved, and the DFO-MSNs are shown to be dispersible under relevant biological conditions and clinically relevant time-scales. Taken together, this makes them promising candidates for longer-term studies of

the biodistribution of MSNs. The MSNs can readily be further functionalized with targeting ligands, and/or other imaging modalities, which also makes the DFO-MSNs interesting for theranostic applications.

Acknowledgements

We like to express our particular gratitude to C. Egger and J. Korzer for their active, friendly and skillfull support of all the experimental work throughout this project.

Electronic Supplementary Information (ESI) available: Elemental, thermogravimetric and nitrogen sorption analyses as well as zeta potential of MSNs, thin layer chromatography and quantitative analysis of ^{89}Zr -DFO-MSNs and biodistribution data in major organs 1 h after intravenous injection. See DOI:

References

1. Q. J. He and J. L. Shi, *Journal of Materials Chemistry*, 2011, **21**, 5845-5855.
2. C. Y. Shi Jian-Lin, Chen Hang-Rong, *Journal of Inorganic Materials*, 2013, **28**, 1-11.
3. F. Tang, L. Li and D. Chen, *Advanced materials*, 2012, **24**, 1504-1534.
4. Y. Kuthati, P.-J. Sung, C.-F. Weng, C.-Y. Mou and C.-H. Lee, *J Nanosci Nanotechno*, 2013, **13**, 2399-2430.
5. V. Mamaeva, C. Sahlgren and M. Linden, *Adv. Drug Delivery Rev.*, 2013, **65**, 689-702.
6. Y. Liu and M. J. Welch, *Bioconjug Chem*, 2012, **23**, 671-682.
7. Q. He, Z. Zhang, F. Gao, Y. Li and J. Shi, *Small*, 2011, **7**, 271-280.
8. X. He, H. Nie, K. Wang, W. Tan, X. Wu and P. Zhang, *Anal Chem*, 2008, **80**, 9597-9603.
9. J. L. Vivero-Escoto, R. C. Huxford-Phillips and W. Lin, *Chem Soc Rev*, 2012, **41**, 2673-2685.
10. J. E. Lee, N. Lee, T. Kim, J. Kim and T. Hyeon, *Acc Chem Res*, 2011, **44**, 893-902.
11. J. M. Rosenholm, V. Mamaeva, C. Sahlgren and M. Linden, *Nanomedicine (Lond)*, 2012, **7**, 111-120.
12. G. Xie, J. Sun, G. Zhong, L. Shi and D. Zhang, *Arch Toxicol*, 2010, **84**, 183-190.
13. R. Kumar, I. Roy, T. Y. Ohulchanskyy, L. A. Vathy, E. J. Bergey, M. Sajjad and P. N. Prasad, *ACS Nano*, 2010, **4**, 699-708.
14. X. Huang, F. Zhang, S. Lee, M. Swierczewska, D. O. Kiesewetter, L. Lang, G. Zhang, L. Zhu, H. Gao, H. S. Choi, G. Niu and X. Chen, *Biomaterials*, 2012, **33**, 4370-4378.
15. F. Chen, H. Hong, Y. Zhang, H. F. Valdovinos, S. Shi, G. S. Kwon, C. P. Theuer, T. E. Barnhart and W. Cai, *ACS Nano*, 2013, **7**, 9027-9039.
16. M. H. Kim, H. K. Na, Y. K. Kim, S. R. Ryoo, H. S. Cho, K. E. Lee, H. Jeon, R. Ryoo and D. H. Min, *ACS Nano*, 2011, **5**, 3568-3576.
17. C. Solbach, J. Bertram, W. Scheel, B. Baur, H. Machulla and S. Reske, *J NUCL MED MEETING ABSTRACTS*, 2013, **54**, 1098-.

18. J. P. Holland, Y. Sheh and J. S. Lewis, *Nucl Med Biol*, 2009, **36**, 729-739.
19. H. C. Wu, J. T. Hsieh, M. E. Gleave, N. M. Brown, S. Pathak and L. W. Chung, *Int J Cancer*, 1994, **57**, 406-412.
20. S. Bhattacharyya and M. Dixit, *Dalton Trans*, 2011, **40**, 6112-6128.
21. X. Huang, L. Li, T. Liu, N. Hao, H. Liu, D. Chen and F. Tang, *ACS Nano*, 2011, **5**, 5390-5399.
22. C. H. Lee, S. H. Cheng, Y. J. Wang, Y. C. Chen, N. T. Chen, J. Souris, C. T. Chen, C. Y. Mou, C. S. Yang and L. W. Lo, *Adv Funct Mater*, 2009, **19**, 215-222.
23. P. Decuzzi, B. Godin, T. Tanaka, S. Y. Lee, C. Chiappini, X. Liu and M. Ferrari, *J Control Release*, 2010, **141**, 320-327.
24. H. Meng, M. Xue, T. Xia, Z. Ji, D. Y. Tarn, J. I. Zink and A. E. Nel, *ACS Nano*, 2011, **5**, 4131-4144.